Jared N. Baucom[1]
Mem. ASME
U.S. Naval Research Laboratory,
Multifunctional Materials Branch,
4555 Overlook Avenue, SW,
Washington, DC 20375

Marriner H. Merrill[2]
Mem. ASME
U.S. Naval Research Laboratory,
Multifunctional Materials Branch,
4555 Overlook Avenue, SW,
Washington, DC 20375
e-mail: marriner.merrill@nrl.navy.mil

Christopher R. Field[3]
U.S. Naval Research Laboratory,
Naval Technical Center for Safety
and Survivability,
4555 Overlook Avenue, SW,
Washington, DC 20375

G. Asher Newsome
Nova Research, Inc.,
1900 Elkin Street, Suite 230,
Alexandria, VA 22308
e-mail: graham.newsome.ctr@nrl.navy.mil

Kevin J. Johnson
U.S. Naval Research Laboratory,
Naval Technical Center for Safety
and Survivability,
4555 Overlook Avenue, SW,
Washington, DC 20375

Effect of Placing a Probe in an Acoustic Drop Levitator

In this paper, we use computational modeling to explore the effects of placing a probe within the active volume of an acoustic levitator. A two-step computational approach is used to visualize the levitation nodes using thousands of simulated particles driven by the acoustophoretic force and gravity. Our analysis shows that the size and position of a probe can strongly alter the shape, location, and intensity of existing levitation nodes. This has a direct impact on the ability to use acoustic levitation for drop suspension in the presence of disruptive probes. [DOI: 10.1115/1.4031672]

Introduction

The use of acoustic forces to levitate and move small objects has been the subject of study for over 40 years [1], and acoustic levitation has been used to suspend a variety of objects, including solids, liquids, and small living specimens [2–4]. Noncontact handling methods are beneficial because they avoid contamination, work for both solid and liquid volumes, and enable manipulation of very small objects [5]. These advantages are particularly important in trace chemical sensing, where interactions between the analyte and the surfaces it encounters during sample handling can significantly impact the sensitivity and precision of the measurement. For example, many explosives are notoriously difficult to work with when using traditional sample handling methods, complicating trace analysis. The lack of such contact also decreases the risk of contamination of the sample holder.

Acoustic levitation must be combined with analytical probes in order to be of greatest benefit. Prior work has investigated coupling an acoustic drop levitator (ADL) with Raman spectroscopy, Fourier transform infrared spectroscopy, gas chromatography, and mass spectroscopy, with significant potential for applications in analytical and bioanalytical chemistry [6–10]. An acoustic levitator is well suited for applications in which the analyte must avoid contact with other surfaces in the experimental apparatus [11,12]. However, these and other applications still require a probe (sampling tube, trace sensor, thermocouple, hot-wire probe, optical lens, etc.) in close proximity to the levitated drop. The objective of this work is to quantify the degree to which the acoustic levitation is affected by the presence of a probe within the active acoustic volume of the levitator.

Physically, acoustic drop levitation is driven by the acoustophoretic force [13,14]. The force can be considered as a transfer of linear momentum from an incident sound wave to the particle. In the limit of a particle much smaller than the wavelength, the radiation force can be derived by considering the contributions from the incident wave and the scattered wave. These are a function both of the acoustic field and the particle itself, particularly the particle size, which directly affects the scattering (reflection) of the wave energy. Particle stiffness can also play a role, but in this case, the particle was assumed to be rigid with no absorption of acoustic energy inside the particle. The interaction of incident, scattered, and absorbed acoustic waves leads to gradient, scattering, and absorption radiation forces that make up the acoustophoretic force.

In the simplest configuration, acoustic levitators create high acoustic pressures and gradients in a standing acoustic wave. An ultrasonic transducer is aimed at a rigid reflector surface. Acoustic waves emitted from the transducer interfere with waves bouncing back from the reflector, and the interference of emitted and reflected waves produces standing waves in which the nodes of zero-pressure appear at discrete locations within the active

[1]Present address: Technetics Group, Columbia, SC 29209.
[2]Corresponding author.
[3]Present address: Field R&D Services, Arlington, VA 22201.

Contributed by the Noise Control and Acoustics Division of ASME for publication in the JOURNAL OF VIBRATION AND ACOUSTICS. Manuscript received March 11, 2015; final manuscript received September 21, 2015; published online October 27, 2015. Assoc. Editor: Nicole Kessissoglou.

acoustic volume. A solid or liquid object in the active acoustic volume is driven by the acoustophoretic force toward these locations of zero acoustic pressure and therefore minimum acoustophoretic force.

The acoustophoretic force balances with other forces (gravity, electrostatic, etc.) to determine the final location of the levitated object. In a simple case, when the acoustophoretic force driving toward a pressure node is balanced by the downward gravitational force on an object, the object is levitated at a position just below the node (shown schematically in Fig. 1).

In our approach, a multiphysics finite element computational model was developed to obtain a detailed understanding of the free-field operational characteristics of the NRL ADL, as well as to predict the effects of an idealized (cylindrical) probe positioned deeply into the active acoustic volume of the ADL. A working acoustic drop levitator was used to experimentally validate the computational model. In Fig. 2, components of the NRL ADL with an idealized probe are shown as the inset, and major dimensions are depicted in the figure.

Our analysis compared different configurations of the simplified geometry shown in Fig. 2. The key differences among the models studied were the presence (or absence) of the probe, its size, and the distance from the centerline of the ADL, which is where the strongest levitation nodes are typically found. The computational model was experimentally validated for the no-probe case with very good agreement between model and experiment. When a probe was present, the model indicated no effect of 20 mm or 10 mm probe-node spacing, but that at 1 mm probe-node spacing, the node was extinguished. The probe also affected the size, location, and shape of other nodes in the ADL. The effect was dependent on probe diameter and on ADL geometry. Semiquantitative data into the node strength (levitating power) were achieved by considering the particle density of the visualization particles in a given node location. The results provide guidance for the specific case of a cylindrical probe deep in the ADL and also a way forward for further modeling of more detailed probe-ADL geometries.

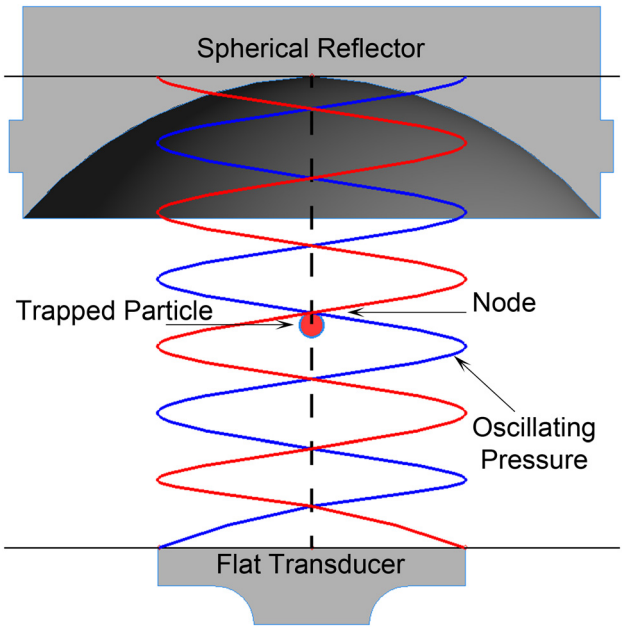

Fig. 1 The distribution of standing axial pressure waves in an acoustic drop levitator depicted as a transverse wave. Nodes along the dashed axis coincide with regions of zero acoustophoretic force, where particles or droplets can be expected to levitate. This schematic assumes a dense particle levitating in a gas phase (the assumed case for a system where a sample is acoustically trapped and then probed).

Methodology

A multiphysics finite element approach was taken to achieve a tight coupling of a stationary solution for the acoustic pressure field with a time-dependent prediction of the motion of uniformly seeded particles within the calculated acoustic pressure field. The computational methodology employed here was designed to visualize the trapping and holding capacity of the levitation nodes. This was done by the calculation of the acoustic pressure distribution within the acoustic volume, followed by tracking the motions of visualization particles released into the volume at the beginning of the time-domain analysis. The particles were subject to gravity, drag, and the acoustophoretic forces obtained from the frequency-domain analysis. Particles that encountered a boundary (hard or soft) were removed from subsequent analysis.

The analysis was performed in two steps. In the first step, the acoustic pressure field was determined by performing an acoustic analysis in the frequency domain. The basic dependent variable in this part of analysis was the pressure distribution within the active volume. Standard assumptions were used for modeling sound propagation in air (e.g., the air was assumed to be an inviscid, homogeneous, isotropic fluid, with constant speed of sound and no acoustic losses).

The computational model was based on the geometry of the experimental ADL shown schematically in Fig. 2. The geometric dimensions and material parameters are given in Table 1. The acoustic input was modeled as an oscillating, hard boundary, which means there were no monopole or dipole acoustic sources, and the problem reduced to an eigenanalysis (Eq. (1)). The solution of this equation yielded the spatial distribution of the pressure extrema. In Eq. (1), p is the acoustic pressure, ρ is the density of air, c is the speed of sound in air, and the eigenvalue ω is proportional to the transducer drive frequency ($\omega = 2\pi f_d$). Three boundary conditions were imposed: (i) sound-hard boundaries on the reflector, (ii) plane-wave radiation at the free (air) boundaries, and (iii) a normal acceleration on the transducer surface. Any probe or obstruction placed in the acoustic volume was also assumed to have a sound-hard boundary

$$-\nabla \cdot \frac{1}{\rho_c}(\nabla p) + \frac{\omega^2 p}{\rho_c c^2} = 0 \tag{1}$$

The second step of the solution was a time-dependent analysis that solved for the motion of thousands of particles seeded uniformly within the active acoustic volume. The particles were initially positioned uniformly throughout the acoustic volume (air) with a particle density of 1000 particles/cm^3, for a total of approximately 42,000 particles for each analysis. The particles

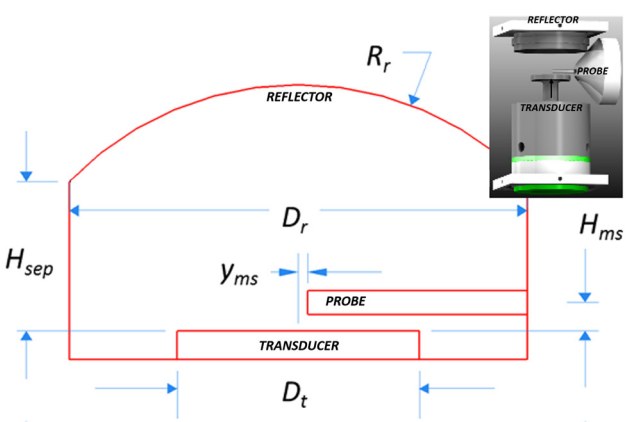

Fig. 2 A basic ADL with an idealized probe inlet (inset). The corresponding model geometry and dimensions are also shown.

started with zero velocity, and their subsequent motion followed Newton's second law [15]. Over time, the particles clustered at the levitating nodes, and the clouds of particles allowed for visualization of the levitating node location, size/shape, and strength. The particles moved in accordance with the conservation of momentum (Eq. (2)) and under the influence of three forces: gravity (Eq. (3)), Stokes' drag (Eq. (4)), and the acoustophoretic force (Eq. (5)), which was derived from the acoustic pressure field computed in the first step of the analysis, the particle velocity, the square of the incident pressure (p_{in}), the square of the incident velocity (v_{in}), particle volume (V_{p}), and functions (f_1 and f_2). The precise forms of the scattering coefficients (f_1 and f_2) are given in Eq. (6) as functions of the density and bulk modulus of the gas and the particle. The angle brackets represent integration over one oscillation period. An explanation of the derivation of Eq. (5) can be found in Ref. [16], with the formulation used in COMSOL and given in Ref. [15]

$$\text{Momentum}: \frac{d(m_p v)}{dt} = \boldsymbol{F}_t \tag{2}$$

$$\text{Gravity}: \boldsymbol{F}_g = m_p \boldsymbol{g} \frac{(\rho_p - \rho)}{\rho_p} \tag{3}$$

$$\text{Stokes' drag}: \boldsymbol{F}_d = \frac{1}{\tau_p} m_p (\boldsymbol{u} - \boldsymbol{v}) \tag{4}$$

$$\text{Acoustophoretic}: \boldsymbol{F}_{\text{acoust}} = -\nabla U^{\text{rad}} = -\nabla\left(V_{\text{p}}\left[f_1 \frac{1}{2\rho c^2}\left\langle p_{\text{in}}^2 \right\rangle - f_2 \frac{3\rho}{4}\left\langle v_{\text{in}}^2 \right\rangle\right]\right) \tag{5}$$

$$\text{Scattering coefficients}: f_1 = 1 - \frac{K_0}{K_p}, \quad f_2 = \frac{2(\rho_p - \rho)}{2\rho_p + \rho} \tag{6}$$

The simulation was allowed to run for 400 ms, though steady-state was reached by about 200 ms. Interparticle forces or collisions were not of interest in this analysis; however, the presence of particles may produce local secondary trap points, as described in Ref. [17]. Particles disappeared when they reached the open simulation boundaries or touched hard surfaces such as the reflector, the transducer, or the probe. These simplifications were used because the purpose of the particles was to identify and visualize the levitation nodes, not to model particle interactions in an ADL.

Computations were performed using a XEON-based personal computer with 32 processing cores and 192 GB of shared memory. COMSOL MULTIPHYSICS 4.3 b was used for three-dimensional (3D) modeling and finite element analysis. The models were spatially discretized using tetrahedral elements and a total of approximately 450,000 degrees-of-freedom (DOF) for the frequency-domain analysis and 130,000 DOF for the time-domain analysis. Computational cost was not an issue for solution of the acoustic field; hence, the number of DOF in the frequency-domain analysis was set to more than four times the number needed for stable solution of the acoustic field. The number of DOF in the time-dependent step was proportional to the number of visualization particles. The number of particles was selected so that nodal locations and shapes could be adequately visualized. Typical solution times were < 5 min for frequency-domain analysis and approximately 10 hrs for time-dependent analysis. For this reason, the parameter space of the computational models was explored to a large extent before committing to time-dependent solutions. Although the large potential computational cost savings of a two-dimensional particle analysis was attractive, it will be shown that the full 3D model yielded results that the two-dimensional model failed to capture.

Table 1 ADL parameters and geometry

Symbol	Value(s)	Description
f_0	33 kHz	Ultrasonic drive frequency
a_0	1.5×10^6 m/s^2	Peak normal acceleration of transducer surface
c_0	343 m/s	Speed of sound in air
D_t	25.4 mm	Transducer diameter
D_r	48.0 mm	Acoustic volume diameter
H_{sep}	15.74 mm	Reflector height
R_r	33.4 mm	Radius of curvature of reflector
d_{MS}	2.5 or 5.0 mm	Probe inlet diameter (assumes values of 2.5 or 5.0 mm)
H_{MS}	3.0 mm	Height of probe inlet centerline above transducer surface
y_{MS}	1, 10, and 20 mm	Probe inlet insertion depth measured from ADL centerline
d_p	$c_0/10f_0$	Diameter of visualization particles
ρ	1.23 kg/m^3	Density of air
ρ_p	500 kg/m^3	Density of each visualization particle
d_v	$2.2\sqrt{1\text{ Hz}/f_0}$ mm	Viscous boundary layer thickness

For the experimental validation, a custom ultrasonic transducer and reflector similar to those described in Ref. [9] were obtained from the Scheeline laboratory at the University of Illinois. It is shown schematically in Fig. 2. The transducer was a simple stepped horn design, with a larger base connected to a thinner horn capped with a radiating plate. Base diameter was 50.4 mm and base height was 60.3 mm tall. The stepped horn diameter was 9.7 mm and it was 15.9 mm tall. On top of this was the radiating plate (25.4 mm diameter and 3.2 mm tall). Total transducer height was 79.4 mm. The stepped design helped to focus and concentrate the power to the radiating plate. The entire transducer was machined out of a single block of aluminum for good acoustic coupling. The transducer was mounted on a miniature optical bench via an x–y stage and a ring mount around its base equipped with plastic-tipped set screws. The reflector was hemispherical, with a radius of curvature of 33.4 mm. It was centered above the transducer and mounted to a motorized actuator (Thorlabs, Newton, NJ, model Z825B) that enabled adjustment of the reflector height above the transducer. The transducer was driven by the output of a sweep function generator (BK Precision, Yorba Linda, CA, model 4017 A) coupled to an RF amplifier (T&C Power Conversion, Inc., Rochester, NY, model AG 1006). In ADL experiments, the function generator was set to provide a 33 kHz sinusoidal signal to the amplifier, which was adjusted to deliver approximately 10 W of power to the transducer. The reflector was positioned at a height of 37 mm above the transducer, which was empirically determined to provide stable levitation at the set frequency.

Results

In this section, we describe the results of our computational models, especially as they relate to the comparison of the effects of presence of probe inlets of different sizes and locations with respect to the primary levitation nodes. The distribution of the acoustic pressure and the final locations of the visualization particles were used as metrics of baseline levitator performance and to quantify the effects of probe intrusion.

The frequency-domain solution for the acoustic distribution is shown in Fig. 3 for the case of an empty acoustic volume with no probe. The results shown are plotted on a central slice at the yz-plane. The model depicted is axisymmetric, so the central nodes are disklike in three dimensions and the shapes of the outer nodes are actually ring shaped. Darker regions in the plot depict zones that oscillate in time between compression and rarefaction. The lighter bands dividing the darker zones are narrow regions in which the acoustic pressure oscillates very close to zero. It is within the lighter bands that we expect objects to be levitated; they are the "levitation nodes." For example, in Fig. 3, four such

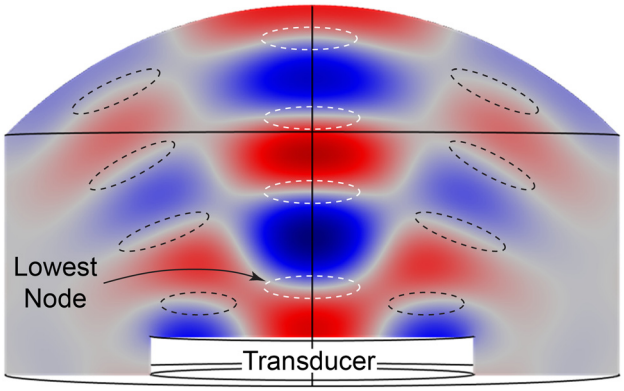

Fig. 3 The acoustic pressure field in the modeled ADL without a probe inlet. White dashed circles show predicted levitation nodes along the axis, and black dashed circles show predicted ring-node levitation.

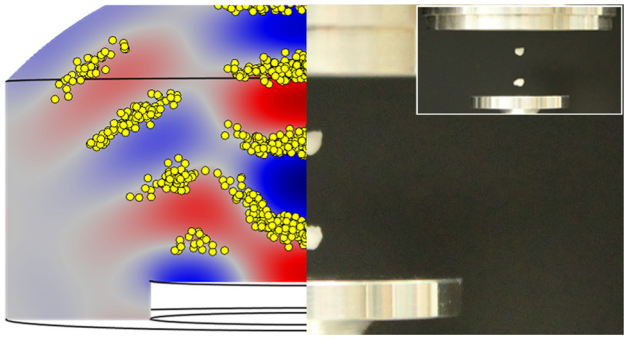

Fig. 5 Experimental validation showing a photograph of the ADL with two levitated beads of foam (right and inset) and the predicted location of the visualization particles after 400 ms. The geometry and driving frequency were the same in each case. Off-axis levitation was also observed experimentally, though the nodes were less stable.

nodes are indicated along the central axis between the transducer surface and the apex of the reflector dome.

In Fig. 4, the final particle locations are shown for the same central slice at the *yz*-plane. These particles were initially dispersed uniformly throughout the active volume, but have collapsed into the levitation nodes within 400 ms of their release. The full 3D particle field can be estimated by rotating these results about the vertical *z*-axis, revealing that the central nodes form the shape of a disk or bowl. The bowl shape is most pronounced in the lowest node of Fig. 4.

For experimental validation, two beads of polystyrene foam were levitated in the NRL ADL. The beads assumed stable positions along the central axis of the levitator. In Fig. 5, a photograph of the levitated foam is placed next to the model predictions and shows an excellent match. As explained above, the model geometry and driving frequency were chosen to replicate the experimental ADL settings used.

A parametric study was carried out to examine the effect of a probe inlet on the acoustic pressure field. The results are shown in Fig. 6. No significant effect of probe size or position was observed at 20 mm or 10 mm from the central axis, but a significant change was observed at 1 mm distance. For the probe with the larger diameter, the central nodes appeared to blend or merge together along the central axis. For both probe diameters, the off-axis nodes became more dominant, as indicated by the higher pressure gradients close to these nodes.

With the addition of a probe, the problem was no longer axisymmetric, and the disruption of axisymmetry was assumed to produce a 3D effect. For this reason, we plot acoustic pressure distributions on two orthogonal planes: the *yz*-plane and the *xz*-plane for the case of a 2.5 mm probe located 1 mm from the centerline (Fig. 7). In Fig. 7, the pressure plot on the left is the same as the bottom/right plot of Fig. 6. The plot on the right of Fig. 7 is rotated by 90 deg about the *z*-axis, and is looking into the probe inlet. The two sectional views of the acoustic pressure field are in stark contrast with each other. The acoustic pressure gradients, which directly relate to the acoustophoretic forces that confine levitated particles within levitation nodes, appear to be higher in the off-axis ring-shaped nodes than they were in the case without a probe.

To further analyze the effect of the probe on the levitation nodes, we examined the modeled particle locations in Fig. 8 and Table 2. The full 3D analysis without (Fig. 8(*a*)) and with (Fig. 8(*b*)) the probe is shown first. The images are roughly isometric in *x*, *y*, and *z*. As previously discussed, the levitation nodes (no-probe case) consist of a series of disk- or bowl-shaped nodes along the axis as well as circumferential ring nodes farther out. When the probe was added (Fig. 8(*b*)), the central nodes became much

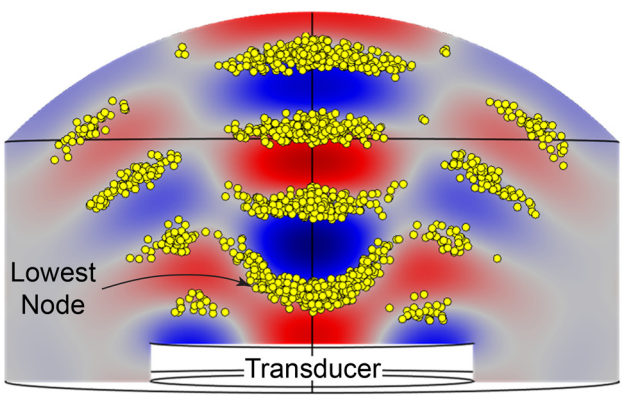

Fig. 4 Visualization particle locations after 400 ms. Particles are shown in a 1 mm-thick slice of the *YZ*-plane. The acoustic pressure field is shown in the background for comparison.

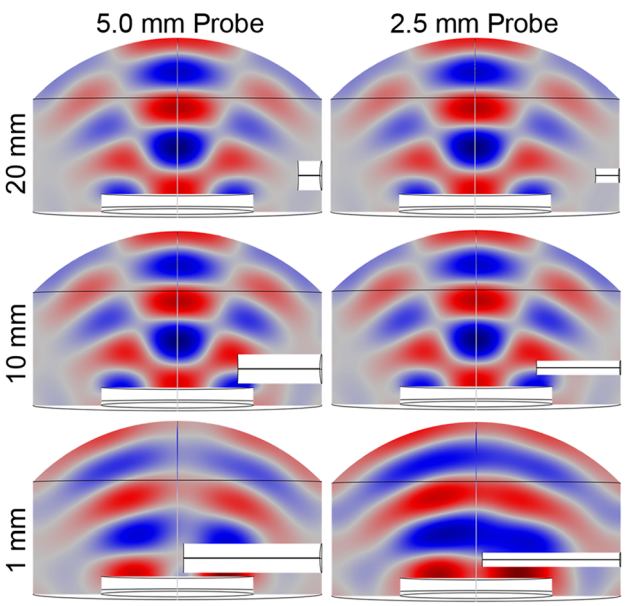

Fig. 6 The effect of probe size and position on the acoustic pressure field is shown for two inlet diameters (5.0 mm on the left and 2.5 mm on the right) and positions (1, 10, and 20 mm from the centerline). The pressure field is shown in the *yz*-plane.

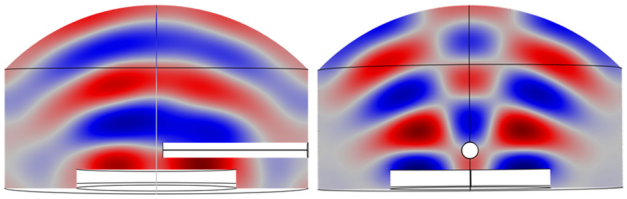

Fig. 7 Two orthogonal views of the pressure distribution for a 2.5 mm probe located 1 mm from the centerline. The two distributions are distinctly different and indicative of the asymmetry caused by the presence of an obstruction in the ADL.

weaker (trapped fewer visualization particles) and the ring nodes split into lobes.

The nodes closest to the probe were isolated by creating a slice 5 mm above the transducer surface. Node data are recorded in Table 2 and the node x–y locations are shown in Fig. 8(*c*). First, for the baseline (no probe) case, we appear to have a strong central node (black) about 4 mm above the transducer as well as a ring (gray) 18 mm in diameter about 2–3 mm above the transducer. While more particles were located in the ring than in the central node, they were much more spread out, and the particle density was highest for the central node. When the case with the probe was considered, there was no central node or ring, but instead three lobes concentrated at 90 deg, 180 deg, and 270 deg with respect to the probe. At first glance, it appears as though the particles that formed the ring node in the no-probe ADL formed the lobes in the ADL with a probe, because approximately the same quantity of particles were involved (951) near the same location. The lobes formed slightly higher than the ring formed (though lower than the central node) and were ~1 mm closer to the central axis than the original ring. Because the particles were split into lobes and not a ring, the local concentration of particles was higher for the lobes compared to the ring node.

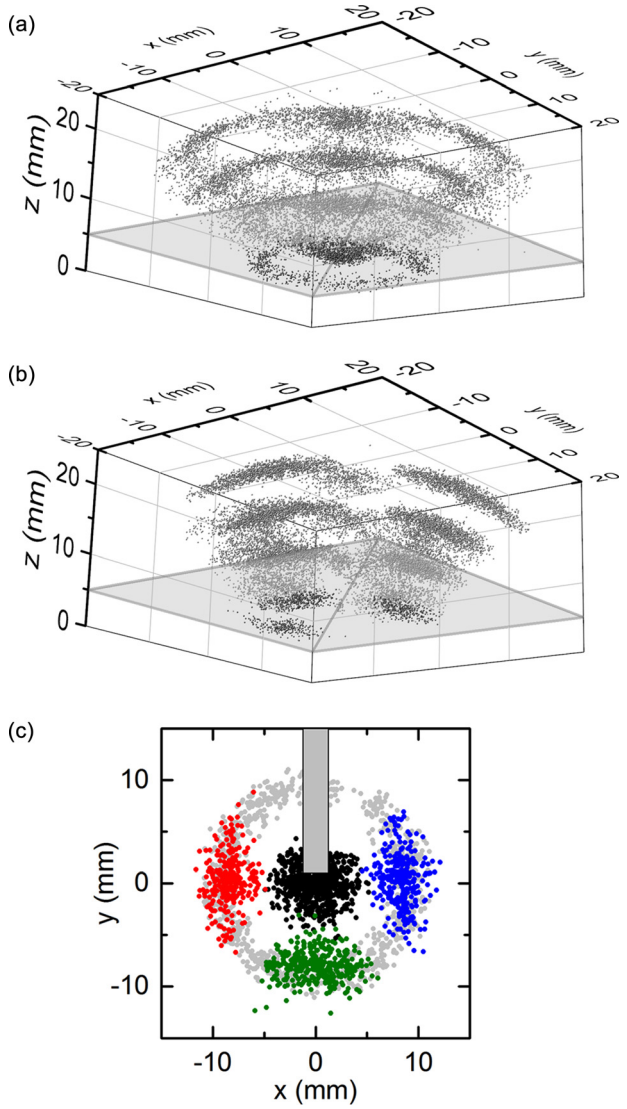

Fig. 8 Visualization particle location without (*a*) and with (*b*) a probe. (*a*) and (*b*) show all particles and indicate the slice taken to focus on the lowest node ($z = 5.5$ mm). In (*c*), the *XY* location of the visualization particles for the lowest node are shown without the probe (gray ring node and black center node) and with the probe (dark gray lobes left, middle, and right).

Table 2 Visualization particle data for nodes in Fig. 8(*c*)

	ADL		ADL + probe		
	Node 1 (black)	Ring 1 (gray)	Lobe 1 (left)	Lobe 2 (middle)	Lobe 3 (right)
Number of particles	790	943	290	369	292
Average distance from center (mm)	0	9.1	8.7	8.4	8.7
Average height (mm)	4.1	2.6	2.9	3.4	3.0

Discussion

The strong correlation between the computational model and experiment indicates the validity of the computational process used. The location and shape of the levitation nodes were computationally predicted by the location and shape of the zero-pressure loci in the acoustic pressure, verified by the equilibrium positions of the visualization particles, and validated experimentally with the NRL ADL using small beads of polystyrene foam (Fig. 5). It is interesting to note that the centroid of the particle cluster (modeled) and the center of each levitated bead (experimental) were found slightly below the zero-pressure nodes from the acoustic analysis in the frequency-domain. This was assumed to be the effect of gravity.

Additionally, the comparative number of visualization particles in a given node provided a semiquantitative indication of which nodes had more trapping or holding strength. The strongest node (greatest number of visualization particles per volume) was predicted to be the node closest to the transducer surface, followed by the next-highest node along the centerline. The prediction was validated experimentally, and we found that the lowest node was consistently the easiest location to achieve levitation of foam beads. Validation of the ringlike nodes was also achieved. A piece of foam was levitated in the lowest ring node, where it was observed to slowly drift around the central axis. Such orbital flight has also been observed in bubbles contained within an acoustically agitated liquid medium [18].

A primary objective of this work was to determine the effects of introducing a probe into the ADL. We modeled the case of a probe in very close proximity to a levitation node because this is a common requirement for many analytical tools. We found that when the probe was positioned within 1 mm of the center, it had the effect of extinguishing the primary levitating node (Fig. 8). The ring node was also extinguished, though three new lobes appeared in approximately the same location. This implies that there is a limiting distance to which a probe can be introduced before levitation is affected. Preliminary experimentation with probes in the experimental ADL was performed with a brass rod of the same dimension as the simulated probe. As predicted, minimal impingement of the acoustic field by the rod did not disrupt levitation. However, efforts to assess the impact of rod placement close to the central axis were confounded by electrostatic

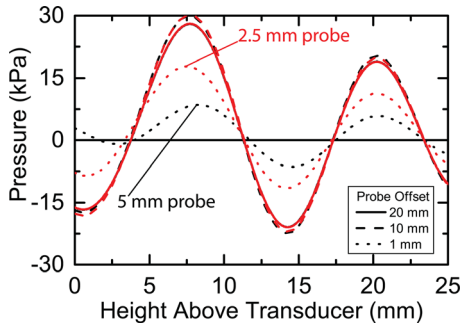

Fig. 9 Acoustic pressure as a function of height above transducer surface along the centerline of the acoustic volume for two probe diameters (5.0 mm and 2.5 mm) and three offset distances (20, 10, and 1 mm). Probe diameter only had a significant effect for the 1 mm case, as indicated.

attraction between the rod and levitated foam beads. Levitation in the ring node was not observed with the rod placed close to the central axis. It should be recognized, of course, that the computational model was concerned with steady-state behavior at fixed geometries, which is somewhat different than seeking to model what would happen to a levitated object while a probe was inserted.

The probe effect appears to be a function of both exact probe dimensions and the ADL geometry. For example, in Fig. 6, we see a less dramatic effect for the smaller diameter probe than for the large-diameter probe (1 mm separation from centerline). The ADL geometry is hypothesized to also have a role by focusing the acoustic pressure. In our case, we used a curved reflector, which acted to focus the acoustic pressures in a rough cone (see Fig. 8(*a*)). At the 3–5 mm height above the transducer, the radius of the outer node (ring node) was about 9–10 mm, which appeared to have been an outer boundary for the probe effect, because placing the probe at 10 mm did not have any significant effect on the pressure field (Fig. 6). If the same simulation had been performed on an ADL with a different geometry or on a different node, there might have been a different behavior because the probe would be farther in (or farther from) the acoustic "cone." This implies that the ADL design can be used to enable reduced probe-sample spacing.

Given the expression for the acoustophoretic force (Eq. (5)), the strength of a levitating node is expected to be a function of the pressure gradients surrounding the node. In Fig. 9, pressure is plotted along the central axis from the transducer surface to the reflector for multiple different ADL cases (baseline and both probe diameters at three different insertions). There is a successive reduction in the magnitude of the pressure peaks as the height above the transducer increases. The reduction of peak pressure produces a commensurate reduction in pressure gradients at the levitation nodes. This implies that the strength of the central levitation nodes decrease as a function of the height above the transducer, as shown both computationally by visualization particles and experimentally.

Two methods to quantify node strength were the visualization particle density and the peak acoustic pressures. Visualization particles (e.g., Fig. 8) gave a qualitative view of the shape and location of the levitation nodes. A more quantitative measure was the particle density, calculated by considering the number of particles in a given volume. Because the particles were modeled without particle–particle interactions and multiple particles were allowed to occupy the same physical space, the particle density was a good indicator of how focused a node was. We observed that there was a good match between dense nodes (computational) and stable levitation (experimental). However, this is still only semiquantitative because the number of particles available to gather at a given node was dependent on the proximity of nodes. For example, two very strong nodes in close proximity would necessarily split the number of available visualization particles and could therefore have a lower density than a weak node with no near neighbors to "share" the available visualization particles. A second quantitative measure was considering the amplitude of the pressure antinodes on either side of the levitation node (Fig. 9). We found that for a probe close to the central node, the peak pressure amplitude decreased by 37% and 70% for the smaller and larger diameter probes, respectively, compared to the no-probe case. These results give some quantification of probe effect at very low computational cost. While this was qualitatively supported by the modeled visualization particles, more work is required in this area, since the acoustophoretic force is not a simple function of pressure amplitude.

Conclusions

We have presented a computational study examining the effect of introducing a probe into an ADL. Acoustic levitation is a useful noncontact method for levitating and moving small objects or drops of liquid. In many instances, the ability to bring a probe into close proximity with the levitated material would add important sensing functionality. However, a probe may also affect levitation. To determine the effect, we modeled an ADL using a two-step technique. First, the acoustic pressure field was solved and then thousands of particles were seeded into the volume and their trajectories tracked under the combined influences of acoustic and gravitational forces. The particles congregated into the levitation nodes within the ADL showing the location, size, and shape of the nodes. Further, the number of particles in a given volume gave a semiquantitative measure of node strength, or its ability to levitate an object. The results of the computational model were validated using a functioning ADL with foam beads levitated in the lowest two axial nodes and showed very good agreement with the computationally predicted clouds of particles.

The modeled results have important implications for inclusion of probes within ADLs. For the geometry considered, the probe showed no significant effect at 20 and 10 mm separation from the levitation node, but at 1 mm spacing, the probe extinguished the node of interest and changed the shape and location of the surrounding levitation nodes. The effect was observed to be more pronounced for the larger probe (5 mm diameter) than for the smaller probe (2.5 mm diameter). We also showed that the curved reflector in the ADL had the effect of focusing the acoustic field and hypothesize that further focusing could allow for closer probe proximity.

The success of this study demonstrates the viability of the computational procedure. It was successfully used to provide a guide in the determination of acoustic levitation, including with obstructions. In future work, more detailed investigation into the critical probe-node spacing should be carried out, as well as a parametric sweep to determine which variables appeared to have the greatest effect at both the lowest node and also in higher nodes that are more centrally located in the acoustic cavity (e.g., probe geometry, spacing, particle properties, and acoustic properties). Future applications will necessitate modeling the effect of more instrument-specific probe geometries, modifications to the ADL (e.g., transducer–reflector spacing or driving frequency), and additional fields, such as would occur with a probe carrying an electrostatic charge. The methodology here shows great promise to provide a straightforward mechanism to carry out these further investigations.

Acknowledgment

Funding for this project was provided by the Office of Naval Research (ONR) through the Basic Research Program of Naval Research Laboratory.

Nomenclature

c = speed of sound in air
f_d = transducer drive frequency

f_1, f_2 = scattering coefficients in acoustophoretic force expression
$\mathbf{F}_d$ = Stokes' drag
$\mathbf{F}_g$ = gravitational force
$\mathbf{F}_t$ = total force acting on a particle
$\mathbf{F}_{acoust}$ = acoustophoretic force
$\mathbf{g}$ = gravitational acceleration
K_i = bulk moduli of particle (K_p) and gaseous medium (K_0)
m_p = particle mass
p = pressure
p_{in} = incident pressure field
$\mathbf{u}$ = fluid velocity
U^{rad} = acoustic radiation potential
$\mathbf{v}$ = particle velocity
v_{in} = incident particle velocity amplitude
V_p = particle volume
ρ = density of medium (air)
ρ_p = density of particle
τ_p = particle velocity response time
ω = eigenvalue of the stationary solution, proportional to drive frequency

References

[1] Santillán, A. O., Boullosa, R. R., and Cutanda-Henriquez, V., 2005, "The Effect of the Geometry of a Resonant Cavity on the Acoustic Levitation Force," Twelfth International Congress on Sound and Vibration, Lisbon, Portugal, July 11–14, pp. 5617–5624.
[2] Sanchez-Salmeron, A. J., Lopez-Tarazon, R., Guzman-Diana, R., and Ricolfe-Viala, C., 2005, "Recent Development in Micro-Handling Systems for Micro-Manufacturing," J. Mater. Process. Technol., **167**(2–3), pp. 499–507.
[3] Xie, W. J., Cao, C. D., Lu, Y. J., Hong, Z. Y., and Wei, B., 2006, "Acoustic Method for Levitation of Small Living Animals," Appl. Phys. Lett., **89**(21), p. 214102.
[4] Park, J. K., and Ro, P. I., 2013, "Noncontact Manipulation of Light Objects Based on Parameter Modulations of Acoustic Pressure Nodes," ASME J. Vib. Acoust., **135**(3), p. 031011.
[5] Vandaele, V., Lambert, P., and Delchambre, A., 2005, "Non-Contact Handling in Microassembly: Acoustical Levitation," Precis. Eng., **29**(4), pp. 491–505.
[6] Alambrok, S., Marston, G., and Pfrang, C., 2013, "Studying Atmospheric Aerosols by Acoustic Levitation: Linking Headspace Solid-Phase Microextraction (HS-SPME) With Gas Chromatography-Mass Spectrometry (GC-MS)," European Aerosol Conference (EAC 2013), Prague, Czech Republic, Sept. 1–6.
[7] Andrade, M. A. B., Buiochi, F., Baer, S., Esen, C., Ostendorf, A., and Adamowski, J. C., 2012, "Experimental Analysis of the Particle Oscillations in Acoustic Levitation," IEEE International Ultrasonics Symposium, Dresden, Germany, Oct. 7–10, pp. 2006–2009.
[8] Brotton, S. J., and Kaiser, R. I., 2013, "Novel High-Temperature and Pressure-Compatible Ultrasonic Levitator Apparatus Coupled to Raman and Fourier Transform Infrared Spectrometers," Rev. Sci. Instrum., **84**(5), p. 055114.
[9] Field, C. R., and Scheeline, A., 2007, "Design and Implementation of an Efficient Acoustically Levitated Drop Reactor for in Stillo Measurements," Rev. Sci. Instrum., **78**(12), p. 125102.
[10] Stindt, A., Albrecht, M., Panne, U., and Riedel, J., 2013, "CO_2 Laser Ionization of Acoustically Levitated Droplets," Anal. Bioanal. Chem., **405**(22), pp. 7005–7010.
[11] Saha, A., Basu, S., Suryanarayana, C., and Kumar, R., 2010, "Experimental Analysis of Thermo-Physical Processes in Acoustically Levitated Heated Droplets," Int. J. Heat Mass Transfer, **53**(25–26), pp. 5663–5674.
[12] Santesson, S., and Nilsson, S., 2004, "Airborne Chemistry: Acoustic Levitation in Chemical Analysis," Anal. Bioanal. Chem., **378**(7), pp. 1704–1709.
[13] Muller, P. B., Barnkob, R., Jensen, M. J. H., and Bruus, H., 2012, "COMSOL Analysis of Acoustic Streaming and Microparticle Acoustophoresis," COMSOL Conference, Milan, Italy, Oct. 10–12.
[14] Silva, G. T., 2014, "Acoustic Radiation Force and Torque on an Absorbing Compressible Particle in an Inviscid Fluid," J. Acoust. Soc. Am., **136**(5), pp. 2405–2413.
[15] COMSOL, 2013, *Particle Tracing Module User's Guide*, COMSOL, Stockholm, Sweden, p. 96.
[16] Barmatz, M., and Collas, P., 1985, "Acoustic Radiation Potential on a Sphere in Plane, Cylindrical, and Spherical Standing Wave Fields," J. Acoust. Soc. Am., **77**(3), pp. 928–945.
[17] Silva, G. T., and Bruus, H., 2014, "Acoustic Interaction Forces Between Small Particles in an Ideal Fluid," Phys. Rev. E: Stat., Nonlinear, Soft Matter Phys., **90**(6), p. 063007.
[18] Shirota, M., Yamashita, K., and Inamura, T., 2012, "Orbital Motions of Bubbles in an Acoustic Field," AIP Conf. Proc., **1474**, pp. 156–159.